

Extracting Forces from Noisy Dynamics in Dusty Plasmas

Wentao Yu,* Jonathan Cho, and Justin C. Burton

Department of Physics, Emory University, Atlanta, Georgia 30322, USA

(Dated: March 9, 2022)

Extracting environmental forces from noisy data is a common yet challenging task in complex physical systems. Machine learning represents a robust approach to this problem, yet is mostly tested on simulated data with known parameters. Here we use supervised machine learning to extract the electrostatic, hydrodynamic, and stochastic forces acting on micron-sized charged particles levitated in an argon plasma. Trained on simulated particle trajectories using more than 100 dynamical and statistical features, the model predicts system parameters with 50% better accuracy than conventional methods, and provides non-contact measurements of the particle charge and Debye length.

Huge amounts of experimental data are often collected faster than can be interpreted. In complex physical or biological systems, this data mostly comes in the form of tracked positions of individual agents or particles, yet random noise makes the inference of internal and external forces challenging. Conventional statistical methods often result in systematic error, and require special treatment of error estimation [1, 2]. Machine learning algorithms can infer forces from trajectories without systematic error [3–9], but their reported performance has been restricted to labeled simulated data rather than unlabeled experimental data. Another restriction is data mismatch [10, 11]. Data is almost always simulated with Gaussian noise, which is presumed in many inference algorithms, but experimental data may include non-Gaussian noise and other artifacts such as systematic drift. Subsequently, modern inference algorithms should be benchmarked using experimental data where parameter estimates can be verified by alternative, independent methods.

Dusty plasmas, where micron-sized charged particles are suspended in a low-density gaseous plasma, provide opportune experimental data for dynamical inference methods. The particles experience a wide array of forces including electrostatic repulsion, hydrodynamic drag from neutral and charged ions, and stochastic thermal kicks [12]. As a result, dusty plasmas display a wide range of complex, nonequilibrium dynamical phenomena, including superthermal excitations from non-reciprocal forces [13–15], oscillations between “turbulent” and “quiescent” states [16–18], parametric resonance and kinetic heating [19–21], spontaneous oscillations at low pressures [22, 23], helical dust “strings” [24, 25], and vortical structure formation at high magnetic fields [26–28]. However, the individual interactions between particles are a subject of active research [29–32], and the external forces acting on a single particle can be complex [22, 33–35]. It is widely believed that particles interact via a screened Coulomb pair potential with parameters Q (particle charge) and λ (Debye length), but these are difficult to measure without disturbing the plasma environment.

Here we show how the undisturbed, random motion

of one and two particles in a dusty plasma can be interpreted using machine learning to provide accurate information about their inter-particle and environmental forces. The supervised machine learning model is trained on extracted features from simulated particle trajectories that consider anisotropic confinement, nonconservative forces, stochastic Lévy noise [36], and experimental drift. In the simulations, the model simultaneously predicts system-wide parameters with 50% better accuracy than traditional methods such as Fourier spectrum and maximum likelihood estimation. In the experiments, one key feature is that many of the inferred parameters can be independently verified by analyzing the particles’ recovery to equilibrium after a perturbation. These results will help guide other studies that use machine learning to quantitatively infer system parameters in real-world, noisy experimental data.

Our experiments used melamine-formaldehyde (MF) particles with diameters $9.46 \pm 0.10 \mu\text{m}$ and $12.8 \pm 0.3 \mu\text{m}$ (microParticles GmbH). The particles were electrostatically levitated in a low-pressure argon plasma above an aluminium electrode with diameter 150 mm (Fig. 1a), similar to previous experiments [16, 22]. In the plasma, the particles become negatively charged with $10^4 - 10^5$ electrons. The argon plasma was generated by a 13.56 MHz radio-frequency voltage applied to the electrode, resulting in $2.9 \pm 0.1 \text{ W}$ of input power and a fixed dc bias voltage of $-36.3 \pm 1.2 \text{ V}$. An aluminium ring was placed on the edge of the electrode to provide horizontal confinement. The plasma pressure, P , was varied between 0.6 Pa and 1.3 Pa. Under these conditions, the typical electron temperature in the plasma was 1.3–1.5 eV [22]. Using 3D tomography, the particles were imaged from above at 50 frames per second with resolution $51 \mu\text{m}$ per pixel in the xy -plane, and $200 \mu\text{m}$ between image slices in z [37]. The 3D particle motion was tracked [38] with corrections accounting for pixel-locking [39]. Without any external perturbations, the particles experienced thermally-excited motion with amplitude $\approx 50\text{--}100 \mu\text{m}$ in the xy -plane (Fig. 1b). Although measurable (Fig. S1), thermal motion in z was much smaller, and was not considered in our machine learning model [37].

Due to the small amplitude of motion, to lowest order, the particles behave as stochastic harmonic oscillators. Let $\vec{r}(t) = x(t)\vec{e}_x + y(t)\vec{e}_y$ denote the two-dimensional (2D) position of a particle at time t , and dotted variables refer to time derivatives. The linearized dynamics of one particle reads:

$$\ddot{\vec{r}} = -\vec{\nabla}\phi + \vec{\nabla} \times \vec{A} - \gamma\dot{\vec{r}} + \vec{N}(\alpha) \quad (1)$$

$$\phi = \frac{\omega^2}{2} [(1 - \delta)(x \cos \theta + y \sin \theta)^2 + (1 + \delta)(-x \sin \theta + y \cos \theta)^2] \quad (2)$$

$$\vec{A} = \frac{k_c}{2}(x^2 + y^2)\vec{e}_z \quad (3)$$

This model contains 6 parameters, γ , ω , δ , θ , k_c , and α . The deterministic confinement force has two components. The conservative potential ϕ resembles a 2D spring characterized by 3 parameters: the average frequency ω , the asymmetry δ between two principal axes, and the angle θ from the x -axis to the weaker principle axis. Two eigenfrequencies, $\omega_- = \omega\sqrt{1 - \delta}$ and $\omega_+ = \omega\sqrt{1 + \delta}$, and θ are displayed in Fig. 1c. The nonconservative vector potential \vec{A} , characterized by a parameter k_c , represents a rotational force possibly due to drag from the background ion flow [40], particle asymmetries [34], or magnetic fields [41]. Additionally, the particle experiences hydrodynamic drag. According to Epstein's law, $\gamma = 0.95P \text{ Pa}^{-1} \text{ s}^{-1}$ [22, 35], where P is the gas pressure. Finally, a stochastic acceleration, $N(\alpha)$, follows a stable Lévy distribution. The parameter α is determined by inference. We do not assume a priori that the stochastic motion is purely Brownian ($\alpha = 2$), and $\alpha < 2$ indicates a more heavy-tailed distribution.

We used the 2D particle time series for the x and y motion (Fig. 1d-e) to infer the 6 model parameters in experiments. Conventional methods, such as maximum likelihood and Fourier transformation, can provide information about *some* parameters with limited accuracy. We incorporate these and other methods as features to train a machine learning model that infers *all* parameters simultaneously with higher accuracy. The features were extracted from simulated time series using the dynamical model (Eqs. 1-3) with 6 random parameters chosen in a given range corresponding to the experiments. The simulated time series varied in length from 150 to 600 seconds, and included both Gaussian and non-Gaussian errors such as drift and pixel-locking from particle tracking [37, 39]. Features were extracted from the time series by two categories of methods. The first category analyzed the two motional degrees of freedom separately by Fourier spectrum, auto-correlation, percentiles, equipartition, intermittency analysis, and velocity distribution. The second category analyzed the entanglement between

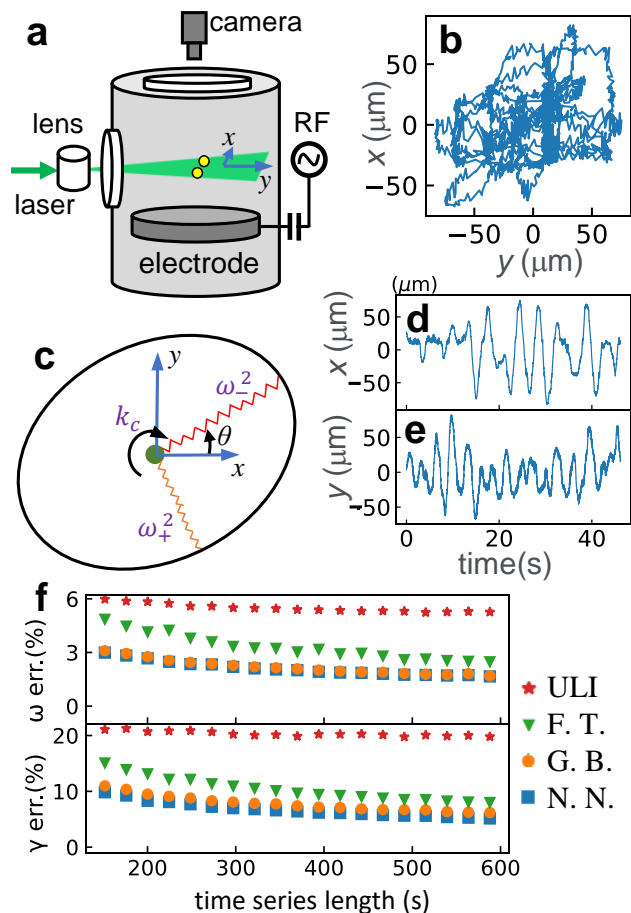


FIG. 1. (a) Diagram of the experimental setup. (b) A trajectory of length 45 s for a single particle undergoing stochastic motion. (c) Linearized external forces on the particle, as described in the text. The black circle represents an equipotential surface of the harmonic confinement. The eccentricity is exaggerated. (d-e) Time series of the x and y position corresponding to the trajectory shown in (b). (f) Percent error from predicting ω (upper panel) and γ (lower panel) by a maximum likelihood method (ULI) [2], Fourier transformation along principal confinement directions (F. T.), Gradient boosting (G. B.) and Neural Network (N. N.). The prediction accuracy for other parameters is shown in Fig. S4a.

the two dimensions by calculating the angular speed, a maximum-likelihood based algorithm [2], and the linear correlation and mutual information between each pair of $x(t)$, $y(t)$, $\dot{x}(t)$, and $\dot{y}(t)$. A detailed explanation of simulating data and feature-extraction is provided in the supplemental information [37].

Two python-based machine learning algorithms (gradient boosting, an ensemble of decision trees, and neural network [42]) were trained on 132 extracted features from 400,000 simulated time series (training data set) to predict the 6 randomly-chosen parameters. The performance of each method was benchmarked on 80,000 simulated time series (test data set). Fig. 1f shows that machine learning methods are $\approx 1.5\times$ more accurate at

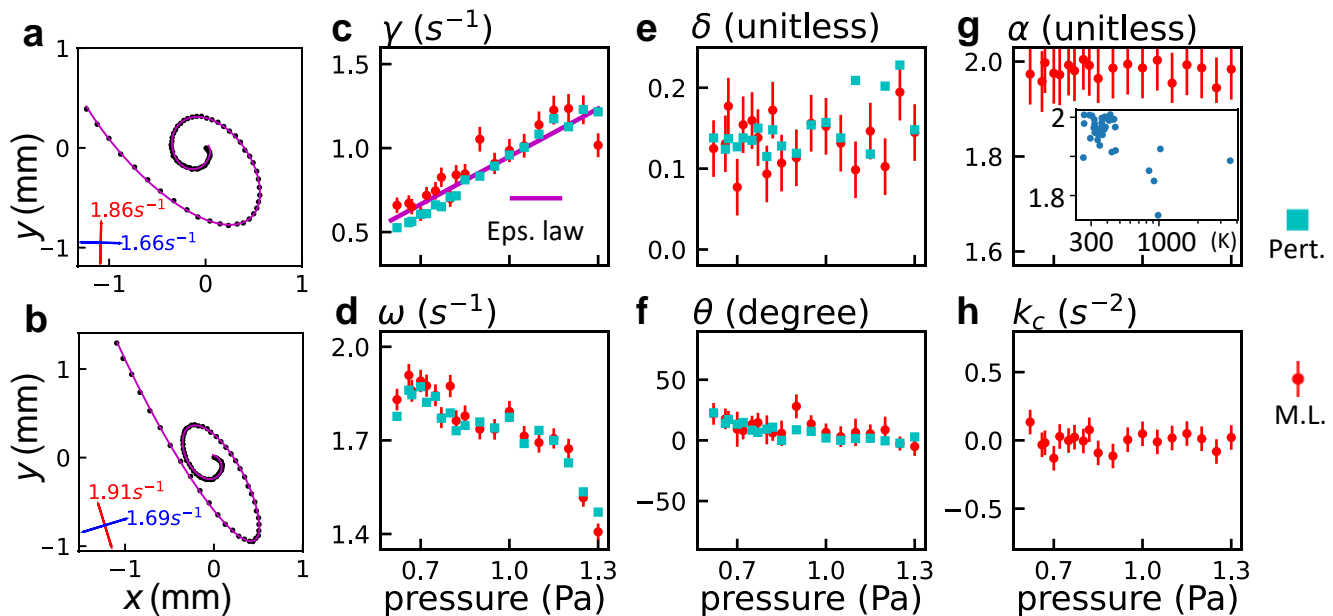


FIG. 2. (a-b) Two different experiments of the same particle relaxing to equilibrium after a perturbation. The pressure was $P = 0.80$ Pa. The magenta lines are fits using Eqs. 1-3 with $k_c = 0$ and no stochastic noise. The red and blue lines indicate ω_+ and ω_- and their orientations, respectively. (c-f) The prediction from the neural network (N.N., red circles) and reference estimation from the perturbation experiments (Pert., cyan square) for γ , ω , δ , and θ . The purple line in (c) represents the theoretical value of Epstein's Law. (g) α and (h) k_c as predicted by the N.N. These parameters cannot be verified by the perturbation experiments. Error bars were obtained from predictions on the simulated test data set, and errors based on fitting perturbed trajectories are smaller and not shown for clarity

predicting ω and γ than simply fitting analytical expressions to the Fourier spectrum of the data along the principal axes of confinement, and $2\text{-}3\times$ more accurate than Underdamped Langevin Inference [2].

It is challenging to verify the accuracy of results when applying machine learning models to unlabeled experimental data. However, in our experiments, we measured the parameters using an independent, alternative method. By perturbing the particle with a magnet outside the chamber and observing the particle's relaxation to equilibrium, we fit the 2D trajectory and obtain estimates of ω , γ , δ , and θ . Assuming $k_c = 0$ and ignoring the stochastic noise term, Eqs. 1-3 can be solved analytically by projecting the motion along the principal axes of external confinement [37]. Two examples of particle trajectories during relaxation to equilibrium after a perturbation, and the corresponding best fit, are shown in Fig. 2a-b.

We directly compare these measurements with the results from the machine learning model, which measures the parameters *in situ* without perturbations. The model estimates the parameters with the same accuracy as the simulated test data set (Fig. 2c-f). In addition, both methods show excellent agreement with the prediction of γ from Epstein's Law. In analyzing the stochastic noise, we found that the prediction of the Lévy parameter α was closely related to the particle's temper-

ature, $2k_B T \approx m\omega^2(\langle x \rangle^2 + \langle y \rangle^2)$, where k_B is Boltzmann's constant (Fig. 2g). Reported values of T in dusty plasmas driven by Brownian motion vary from 300-1000 K [21, 43]. For most experiments, we found $T = 300 - 460$ K, with $1.9 < \alpha < 2$, indicating nearly Gaussian noise (Fig. 2g, inset). Larger temperatures always corresponded to smaller values of α , possibly due to undetectable, nanoscopic dust also levitated in the system rather than the purely Brownian noise. Therefore we excluded data with larger temperatures from all panels in Fig. 2. Importantly, no information about the temperature was passed to the machine learning model since all time series were normalized [37]. The non-conservative force from Eq. 3 was consistent with $k_c = 0$ for most experiments. Larger deviations from zero were accompanied by smaller values of α and larger temperatures.

When two particles are present, their mutual repulsion, $m\vec{f}_{ij} = m f_p(r)\vec{e}_{ij}$, displaces them from the center of the confining potential, as shown in Fig. 3a. Here, f_p is the reduced force, \vec{e}_{ij} is a unit vector from particle i to j , r is the particle separation, and m is the mass of a particle. At equilibrium, the particle separation is r_0 . Here we aim to simultaneously infer $\frac{df_p}{dr}|_{r=r_0} = \omega_p^2$, $f_p(r_0) = \omega_-^2 \frac{r_0}{2}$, and all other model parameters from Eqs. 1-3 with high accuracy using noisy data. We linearize the small-amplitude motion of each particle about their equilibrium position.

The equation of motion for particle i is:

$$\ddot{\mathbf{r}}_i = -\vec{\nabla}\phi + \vec{\nabla} \times \vec{\mathbf{A}} - \vec{\mathbf{f}}_{ij} - \gamma\dot{\mathbf{r}}_i + \vec{\mathbf{N}}(\alpha), \quad (4)$$

$$\vec{\mathbf{f}}_{ij} = f_p \vec{\mathbf{e}}_{ij} = \left(-\omega_p^2(r - r_0) + \omega^2(1 - \delta) \frac{r_0}{2} \right) \vec{\mathbf{e}}_{ij}. \quad (5)$$

The equilibrium force and its differential can be used to solve for 2 independent parameters in a model for f_p . The most commonly used model for f_p assumes a screened, Coulomb interaction:

$$F_D = m f_D = \frac{Q^2}{4\pi\epsilon r} \left(\frac{1}{r} + \frac{1}{\lambda} \right) e^{-r/\lambda}. \quad (6)$$

With this assumption, similar linearized models have been used to directly infer Q and λ from the one-dimensional motion of two particles using Fourier analysis [29, 30, 44, 45]. Here we allow for entanglement between motion in two dimensions, and provide estimates of all model parameters. Analogous to the single particle model, parameters γ , ω , δ , θ , k_c , α , and ω_p were randomly chosen to simulate time series using Eqs. 2-5. The same feature extraction methods as described for a single particle were applied to the center of mass and relative coordinates, $(\vec{\mathbf{r}}_1 + \vec{\mathbf{r}}_2)/2$ and $\vec{\mathbf{r}}_1 - \vec{\mathbf{r}}_2$ [37]. The neural network and gradient boosting models were trained on 227 extracted features from 400,000 simulated time series to predict the 7 parameters, and their performance on simulated test data is shown in Fig. S4b.

The equilibrium separation r_0 and height of the particles were directly measured in experiments (Figs. 3b-c). In particular, below $P \approx 1$ Pa, r_0 sharply increased to a plateau and the height increased, presumably due to an increase in the plasma Debye length. This variation in the plasma environment is evident in some estimated parameters. While γ varies linearly with P and agrees with Epstein's law (Fig. 3d), ω and ω_p show non-monotonic variation with pressure (Fig. 3e). The variation of δ and k_c are shown in Fig. S5, as well as all data for a system of two 9.46 μm particles [37].

To estimate Q and λ , we used two models for f_p . The first is Eq. 6, and the second model is derived from a potential ($m f_w = -d\phi_w/dr$) that incorporates the virtual charge from the ion wake beneath each particle [18]:

$$\phi_w = \frac{Q^2}{4\pi\epsilon\lambda} \left[\frac{e^{-r/\lambda}}{r/\lambda} - \tilde{q} \frac{\lambda e^{-r_w/\lambda}}{r_w + b\lambda e^{-r_w/\lambda}} \right]. \quad (7)$$

Here $r_w = \sqrt{r_0^2 + 0.12\lambda^2}$, $\tilde{q} = 0.3$, and $b = 1$. The predictions of Q and λ differ by only 10%, as shown in Fig. 3f-g. We expect this difference to be much larger if the particles have significant vertical separation, where ion wake forces lead to non-reciprocal forces [14]. It is also important to note that the error in estimating Q and λ can be up to $10\times$ larger than ω (Fig. 3), emphasizing the importance of accurate estimation of all parameters, independent of the model chosen for f_p .

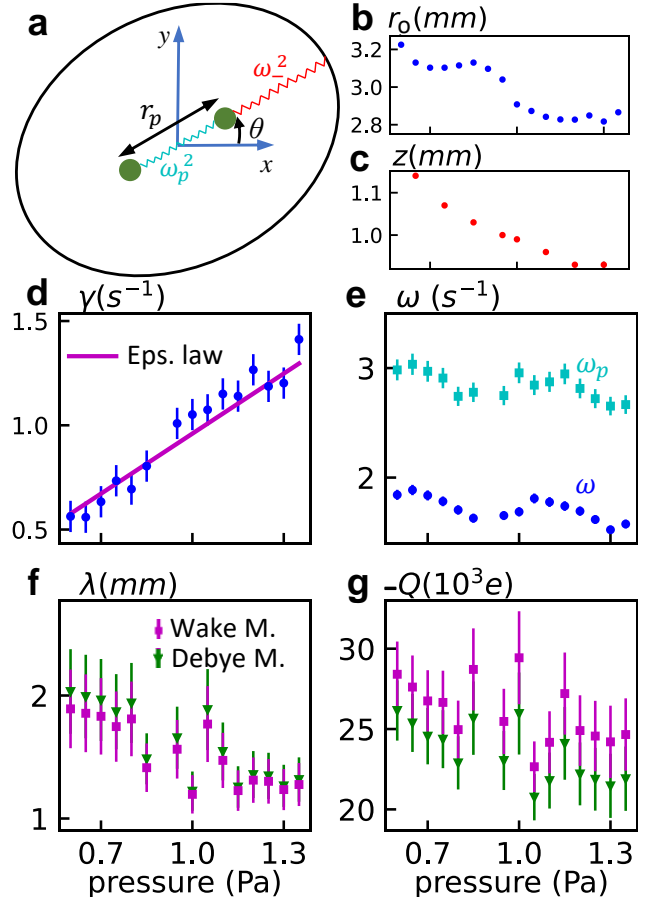


FIG. 3. (a) Two charged particles experience mutual repulsion, characterized by frequency ω_p at equilibrium, and external harmonic confinement. k_c and ω_+ are omitted for clarity. All subsequent panels show parameter estimates as a function of pressure, P . (b-c) The equilibrium particle separation and vertical height above the electrode. (d) Neural network prediction of γ , where the line represents Epstein's law. (E) Particle interaction frequency, ω_p , and the confinement frequency, ω . Error bars are obtained by prediction on the simulated test data set. Note that the eigenfrequency of the relative motion is $\sqrt{2\omega_p^2 + \omega^2}$. (f-g) The Debye length λ and particle charge Q obtained from the Debye model (Eq. 6, green triangle) and the particle wake model (Eq. 7, magenta square).

In conclusion, we have overcome two major restrictions when inferring parameters from experimental data with machine learning: data labeling and mismatch. In our dusty plasma experiments, we label our data by observing particles' relaxation after perturbation, and alleviate mismatch by including non-Gaussian noise and drift in simulated data. This provides simultaneous and accurate estimates of multiple parameters from noisy data, and is essential for an accurate in-situ determination of the particle charge and Debye length in dusty plasmas. In dynamical systems with many particles, often the interaction force cannot be linearized, and a good model may not be obvious. This universal problem remains an

open challenge for dynamical inference.

We thank Ilya Nemenman and Guram Gogia for stimulating discussions. This material is based upon work supported by the National Science Foundation under Grant No. 2010524.

* wentao.yu@emory.edu

- [1] B. Lehle and J. Peinke, *Phys. Rev. E* **91**, 062113 (2015).
- [2] D. B. Brückner, P. Ronceray, and C. P. Broedersz, *Phys. Rev. Lett.* **125**, 058103 (2020).
- [3] J. Bongard and H. Lipson, *P. Natl. Acad. Sci. USA* **104**, 9943 (2007).
- [4] K. Champion, B. Lusch, J. N. Kutz, and S. L. Brunton, *Proceedings of the National Academy of Sciences* **116**, 22445 (2019).
- [5] S. L. Brunton, J. L. Proctor, and J. N. Kutz, *P. Natl. Acad. Sci. USA* **113**, 3932 (2016).
- [6] B. C. Daniels and I. Nemenman, *Nat. commun.* **6**, 1 (2015).
- [7] B. Lusch, J. N. Kutz, and S. Brunton, *Nat. Commun.* **9**, 4950 (2018).
- [8] V. Bapst, T. Keck, A. Grabska-Barwińska, C. Donner, E. D. Cubuk, S. S. Schoenholz, A. Obika, A. W. Nelson, T. Back, D. Hassabis, *et al.*, *Nat. Phys.* **16**, 448 (2020).
- [9] J. Pathak, B. Hunt, M. Girvan, Z. Lu, and E. Ott, *Phys. Review. Lett.* **120**, 024102 (2018).
- [10] E. Vincent, S. Watanabe, A. A. Nugraha, J. Barker, and R. Marxer, *Comput. Speech Lang.* **46**, 535 (2017).
- [11] J. Wang, G. Gui, and H. Sari, *Phys. Commun.* **48**, 101428 (2021).
- [12] M. Chaudhuri, A. V. Ivlev, S. A. Khrapak, H. M. Thomas, and G. E. Morfill, *Soft Matter* **7**, 1287 (2011).
- [13] T. Bockwoldt, O. Arp, K. O. Menzel, and A. Piel, *Phys. Plasmas* **21**, 103703 (2014).
- [14] A. V. Ivlev, J. Bartnick, M. Heinen, C.-R. Du, V. Nosenko, and H. Löwen, *Phys. Rev. X* **5**, 011035 (2015).
- [15] K. Qiao, J. Kong, L. S. Matthews, and T. W. Hyde, *Phys. Rev. E* **91**, 053101 (2015).
- [16] G. Gogia and J. C. Burton, *Phys. Rev. Lett.* **119**, 178004 (2017).
- [17] G. Gogia, W. Yu, and J. C. Burton, *Phys. Rev. Research* **2**, 023250 (2020).
- [18] N. P. Kryuchkov, L. A. Mistryukova, A. V. Sapelkin, and S. O. Yurchenko, *Phys. Rev. E* **101**, 063205 (2020).
- [19] J. D. Williams and E. Thomas Jr., *Phys. Plasmas* **14**, 0637021 (2007).
- [20] G. E. Norman and A. V. Timofeev, *Phys. Rev. E* **84**, 056401 (2011).
- [21] J. Kong, K. Qiao, L. S. Matthews, and T. W. Hyde, *J. Plasma Phys.* **82**, 905820505 (2016).
- [22] J. Méndez Harper, G. Gogia, B. Wu, Z. Laseter, and J. C. Burton, *Phys. Rev. Research* **2**, 033500 (2020).
- [23] S. Nunomura, T. Misawa, N. Ohno, and S. Takamura, *Phys. Rev. Lett.* **83**, 1970 (1999).
- [24] J. Kong, T. W. Hyde, L. Matthews, K. Qiao, Z. Zhang, and A. Douglass, *Phys. Rev. E* **84**, 016411 (2011).
- [25] T. W. Hyde, J. Kong, and L. S. Matthews, *Phys. Rev. E* **87**, 053106 (2013).
- [26] M. Choudhary, R. Bergert, S. Mitic, and M. H. Thomas, *Phys. Plasmas* **27**, 063701 (2020).
- [27] M. Schwabe, U. Konopka, P. Bandyopadhyay, and G. E. Morfill, *Phys. Rev. Lett.* **106**, 215004 (2011).
- [28] E. Thomas Jr., U. Konopka, R. L. Merlino, and M. Rosenberg, *Phys. Plasmas* **23**, 055701 (2016).
- [29] T. E. Sheridan, M. R. Katschke, and K. D. Wells, *Rev. Sci. Instrum.* **78**, 023502 (2007).
- [30] A. K. Mukhopadhyay and J. Goree, *Phys. Rev. Lett.* **109**, 165003 (2012).
- [31] Z. Ding, J. Yao, Y. Wang, C. Yuan, Z. Zhou, A. Kudryavtsev, R. Gao, and J. Jia, *Plasma Sc. Technol.* (2021).
- [32] M. Lampe, G. Joyce, and G. Ganguli, *Phys. Plasmas* **7**, 3851 (2000).
- [33] A. Melzer, in *Physics of Dusty Plasmas* (Springer Nature, Switzerland AG, 2019) pp. 31–57.
- [34] V. Nosenko, F. Luoni, A. Kaouk, M. Rubin-Zuzic, and H. Thomas, *Phys. Rev. Research* **2**, 033226 (2020).
- [35] A. Melzer and J. Goree, in *Low temperature plasmas fundamentals, technologies, and techniques*, Vol. 1, edited by R. Hippler, H. Kersten, M. Schmidt, and K. H. Schoenbach (Wiley-VCH, 2008) 2nd ed., pp. 157–206.
- [36] P. Levy, *Lévy Théorie de l'addition des variables aléatoires* 1937 (1954).
- [37] See Supplemental Material at [URL will be inserted by publisher] for a detailed description of the experiments and simulations.
- [38] D. B. Allan, T. Caswell, N. C. Keim, C. M. van der Wel, and R. W. Verweij, “soft-matter/trackpy: Trackpy v0.5.0,” (2021).
- [39] S. Burov, P. Figliozzi, B. Lin, S. A. Rice, N. F. Scherer, and A. R. Dinner, *P. Natl. Acad. Sci. USA* **114**, 221 (2017).
- [40] K.-B. Chai and P. M. Bellan, *Phys. Plasmas* **23**, 023701 (2016).
- [41] U. Konopka, D. Samsonov, A. V. Ivlev, J. Goree, V. Steinberg, and G. E. Morfill, *Phys. Rev. E* **61**, 1890 (2000).
- [42] F. Pedregosa, G. Varoquaux, A. Gramfort, V. Michel, B. Thirion, O. Grisel, M. Blondel, P. Prettenhofer, R. Weiss, V. Dubourg, J. Vanderplas, A. Passos, D. Cournapeau, M. Brucher, M. Perrot, and E. Duchesnay, *J. Mach. Learn. Res.* **12**, 2825 (2011).
- [43] M. Himpel and A. Melzer, *Phys. Rev. E* , 063203 (2019).
- [44] K. Qiao, Z. Ding, J. Kong, M. Chen, L. S. Matthews, and T. W. Hyde, arXiv preprint arXiv:1705.01982 (2017).
- [45] J. Kong, K. Qiao, L. S. Matthews, and T. W. Hyde, *Phys. Rev. E* **90**, 013107 (2014).